Precapillary sphincters and pericytes at first-order capillaries as key regulators for brain capillary perfusion

Stefan Andreas Zambach[a,1], Changsi Cai[a,1,2], Hans Christian Cederberg Helms[b], Bjørn Olav Hald[a], Yiqiu Dong[c], Jonas Christoffer Fordsmann[a], Reena Murmu Nielsen[a], Jingshi Hu[c], Micael Lønstrup[a], Birger Brodin[b], and Martin Johannes Lauritzen[a,d,2]

[a]Department of Neuroscience, Faculty of Health and Medical Science, University of Copenhagen, 2200 Copenhagen, Denmark; [b]Department of Pharmacy, University of Copenhagen, 2200 Copenhagen, Denmark; [c]Department of Applied Mathematics and Computer Science, Technical University of Denmark, 2800 Kgs. Lyngby, Denmark; and [d]Department of Clinical Neurophysiology, Rigshospitalet, 2100 Copenhagen, Denmark

Edited by Marcus E. Raichle, Washington University in St. Louis, St. Louis, MO, and approved April 15, 2021 (received for review November 16, 2020)

Rises in local neural activity trigger local increases of cerebral blood flow, which is essential to match local energy demands. However, the specific location of microvascular flow control is incompletely understood. Here, we used two-photon microscopy to observe brain microvasculature in vivo. Small spatial movement of a three-dimensional (3D) vasculature makes it challenging to precisely measure vessel diameter at a single x–y plane. To overcome this problem, we carried out four-dimensional (x–y–z–t) imaging of brain microvessels during exposure to vasoactive molecules in order to constrain the impact of brain movements on the recordings. We demonstrate that rises in synaptic activity, acetylcholine, nitric oxide, cyclic guanosine monophosphate, ATP-sensitive potassium channels, and endothelin-1 exert far greater effects on brain precapillary sphincters and first-order capillaries than on penetrating arterioles or downstream capillaries, but with similar kinetics. The high level of responsiveness at precapillary sphincters and first-order capillaries was matched by a higher level of α-smooth muscle actin in pericytes as compared to penetrating arterioles and downstream capillaries. Mathematical modeling based on 3D vasculature reconstruction showed that precapillary sphincters predominantly regulate capillary blood flow and pressure as compared to penetrating arterioles and downstream capillaries. Our results confirm a key role for precapillary sphincters and pericytes on first-order capillaries as sensors and effectors of endothelium- or brain-derived vascular signals.

pericytes | vascular smooth muscle | arterioles | capillaries | neurovascular coupling (NVC)

Variations in neuronal activity trigger robust changes in brain metabolism and perfusion. This relationship is exploited by functional neuroimaging techniques that use changes in cerebral blood flow (CBF) or the blood-oxygenation-level-dependent signal to track brain function (1). The structural basis for local CBF control is the neurovascular unit, which comprises neurons, astrocytes, vascular mural cells, endothelial cells, and components of the extracellular matrix (2–4). The term "neurovascular coupling" (NVC) denotes the robust regulation of CBF that accompanies changes in brain activity in order to match energy demands. Disruption of NVC is a key characteristic of neurologic diseases, e.g., Alzheimer's disease (5), stroke (6) and subarachnoid hemorrhage (7). Therefore, there is an urgent need to understand NVC mechanisms.

Vascular smooth muscle cells (VSMCs) encircle brain arteries and arterioles, representing a key mechanism of cerebrovascular resistance, and pericytes on adjacent capillaries may serve a similar regulatory function (8, 9), but this is incompletely understood. There is an ongoing debate in the field about how to distinguish pericytes from VSMCs and precapillary arterioles from capillaries. Particularly, vascular mural cells demonstrate distinct phenotypes at different capillary locations, with respect to transcriptomes and morphologies (*SI Appendix*, Fig. S1) (10–12). In this study, we used the unbiased, unambiguous vascular branch order as a backbone to identify the specific location of microvascular control. Moreover, small spatial movement of a three-dimensional (3D) vasculature makes it challenging to precisely measure vessel diameter at a single x–y plane. To overcome this problem, we used a four-dimensional (4D) (x–y–z–t) two-photon imaging protocol that minimized the spatiotemporal variance of vessel positions during the experiments, which included exposure to vasoactive drugs that changed the diameter of the sample.

Novel findings suggest that precapillary sphincters and pericytes on the first few branches of capillaries may produce larger and faster vascular diameter responses than VSMCs on arteries and arterioles (8, 9, 13–15). Pericyte loss results in disruption of NVC (16), but it is unknown whether these findings can be generalized. The present study examined this hypothesis. We investigated endothelium-derived factors, because endothelial pathways are involved in functional NVC (17), possibly via *N*-methyl-D-aspartate receptors (18) and retrograde hyperpolarization via $K_{ir}2.1$ channels (19, 20) on capillary endothelial cells, as well as Caveolin1 and nitric oxide synthase (NOS) on arteriolar endothelial cells (4). We also examined ATP-sensitive potassium (K_{ATP}) channels, which are

Significance

Rises in local brain activity are accompanied by increases in blood perfusion, a process known as neurovascular coupling. This relationship constitutes the physiological basis of functional neuroimaging scans, but the exact mechanisms are unknown. Using four-dimensional (x–y–z–t) two-photon imaging, we examined the responsivity from arterioles to capillaries to a suite of vasoactive molecules. Our data indicated that the responsiveness of precapillary sphincters and first-order capillaries was much higher than for the other vessel segments. Our results suggest that precapillary sphincters and pericytes on first-order capillaries are key sensors and effectors of capillary control and an important part of the complex set of mechanisms that regulate cerebral blood flow.

Author contributions: C.C., B.B., and M.J.L. designed research; S.A.Z., C.C., H.C.C.H., B.O.H., J.C.F., R.M.N., and M.L. performed research; Y.D. and J.H. contributed new reagents/analytic tools; S.A.Z., C.C., H.C.C.H., B.O.H., and J.C.F. analyzed data; and S.A.Z., C.C., H.C.C.H., and M.J.L. wrote the paper.

The authors declare no competing interest.

This article is a PNAS Direct Submission.

Published under the PNAS license.

[1]S.A.Z. and C.C. contributed equally to this work.

[2]To whom correspondence may be addressed. Email: ccai@sund.ku.dk or mlauritz@sund.ku.dk.

This article contains supporting information online at https://www.pnas.org/lookup/suppl/doi:10.1073/pnas.2023749118/-/DCSupplemental.

Published June 21, 2021.

highly enriched in pericytes and may contribute critically to capillary flow regulation and NVC (21, 22).

Our first objective was to examine the involvement of acetylcholine (Ach), nitric oxide (NO), K_{ATP} channels, and endothelin-1 (ET1) signaling in regulation of blood flow in brain capillaries in the resting state, during activity increases, and in cardiac arrest. Our second objective was to identify whether the pericyte signaling pathways involved in NO- or K_{ATP}-mediated relaxation and ET1-induced constriction was the same as in VSMCs in order to confirm similar second messenger pathways in VSMCs and pericytes. Our findings suggest that vasoactive signaling molecules modulate VSMCs, precapillary sphincters, and contractile pericytes of the first order of capillaries with the same kinetics, but with the largest diameter responses colocalizing with precapillary sphincters and pericyte cell bodies at first-order capillaries. Modeling results confirmed our experimental data and indicated that variations in pericyte contraction at precapillary sphincters and first-order capillaries play a key role for NVC and for the regulation of brain microvascular resistance and flow in response to the most common vascular signaling molecules.

Results

We used in vivo 4D (x–y–z–t) two-photon microscopy to examine the regulation of microvascular flow in anesthetized NG2dsRed mice (Fig. 1 *A* and *B*), which express a red fluorescent protein in pericytes (in red, Fig. 1*C*) and in VSMCs (23). We identified a precapillary sphincter at the joint of penetrating arteriole (PA) and capillary, as well as its indentation morphology with thick enwrapping of contractile mural cells (Fig. 1*C*). We defined capillaries by their branching order, with first order being the first capillary branching from the PA, and so on (Fig. 1*C*). To minimize focus drift of in vivo two-photon microscopy, we implemented fast and repetitive 4D imaging (x–y–z–t). For every session, we recorded a z-stack consisting of 10 to 14 images per second, including image planes above and below the primary imaging plane. By this procedure, we could minimize deviations in the sample position between consecutive imaging sessions and improve the conditions for dynamic in vivo studies in order to eliminate the influence of vessel movements on diameter assessment. It is particularly a necessity to study precapillary sphincters, which have a small diameter and short length, and therefore are easily lost to focus changes during imaging (*SI Appendix*, Fig. S2). Note that the temporal resolution was approximately one frame per second at any given imaging plane, and our 4D imaging approach is not suitable for tracking fast brain activities, e.g. neuronal signals. A glass micropipette was inserted in proximity to the PAs, precapillary sphincters, and the first- to third-order capillaries for local pressure ejection (puff) of vasoactive compounds and for recording of local field potentials (Fig. 1 *A*–*C*) (9, 24). Whisker pad (WP) stimulation was used for NVC studies (8, 9, 15).

To examine pericyte responses to vasodilatory and contractile signals, we imaged diameter changes of PAs, precapillary sphincters, and first- to third-order capillaries in vivo after local delivery of vasodilator or vasoconstrictive compounds. We monitored diameter changes rather than red blood cell velocity and flux because capillary diameter changes reflect mainly local responses, while changes in the local red blood cell velocity may reflect events occurring in both up- and downstream segments of the microvascular bed (25).

Ach-Induced Vasodilation Is Mediated by NO Synthesis in Capillary Endothelium. Pericytes engage in several types of surface contact with capillary endothelial cells, including gap and adherens junctions and peg–socket junctions (26). Besides, pericytes are within diffusion range of endothelial-derived NO. This proximity of endothelial cells and pericytes led us to examine the possibility of an endothelial influence on the capillary diameter. First, we examined the role of endothelial-derived NO for capillary vasodilation. For this purpose, we recorded capillary diameter changes in response

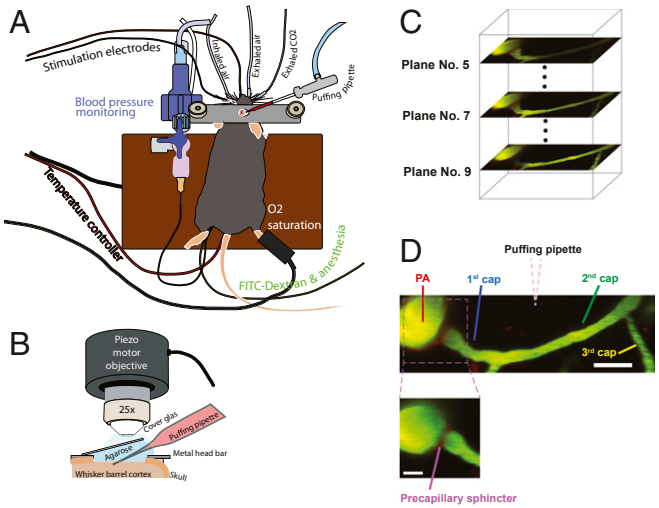

Fig. 1. Diagram of the in vivo experimental setup. (*A*) The physiological state of the mouse was monitored throughout the experiment, including arterial blood pressure, exhaled CO_2, body temperature, heart rate, and O_2 saturation. Vessel lumen dye FITC-dextran and anesthesia alpha-chloralose were infused via a femoral vein catheter. Two stimulations are implemented: WP stimulation and a microglass pipette inserted into the imaging area for local ejection (puff). (*B*) The puffing micropipette is placed in proximity to the arteriole–capillary site, containing 10 μM Alexa 594 and vasoactive compound to visualize the pipette tip as red under the fluorescent microscope. The 25× objective with a piezo motor is used to facilitate fast time-lapse 3D imaging. (*C*) A representative two-photon image stack with different plane focusing on different vessel segments. We performed 4D imaging (x–y–z–t) to precisely focus and measure vessel diameters. The temporal resolution was approximately one z-stack per second. (*D*) An average of two-photon image stack recorded at different depths, with red indicating pericytes and green indicating the vessel lumen. Capillaries are classified as the branching order from the PA, precapillary sphincter, first-order capillary (1st cap), second-order capillary (2nd cap), and third-order capillary (3rd cap). The dashed pink lines indicate the pipette tip. (Scale bar, 20 μm.) (*Inset*) An enlarged precapillary sphincter, showing its indentation lumen and thick embracement of mural cells. (Scale bar, 10 μm.)

to local puffing of Ach (25), which activates the constitutive endothelial NO synthase (eNOS), causing NO release (27–29). Puffing of 2 mM Ach consistently induced vasodilation at PA, the precapillary sphincter, and of capillaries with the largest diameter change at precapillary sphincter. In comparison, intravenous (i.v.) bolus infusion of the NOS inhibitor NG-nitro-L-arginine methyl ester (L-NAME) at a dosage of 30 mg/kg blocked the response at PA, precapillary sphincter, and first- and second-order capillaries (Fig. 2 *A*–*C*). This result is consistent with NO's being a main contributor to Ach-induced VSMC and pericyte relaxation.

To investigate whether rises in NOS activity influence NVC, we used an i.v. bolus injection of L-NAME and assessed the dilation peak, half-peak duration evoked by WP stimulation. The NVC responses remained unchanged in response to systemic L-NAME, suggesting that NO under our stimulation conditions do not contribute to NVC (Fig. 2 *D*–*F*). L-NAME also had no effect on response amplitudes and latencies in WP-induced field excitatory postsynaptic potential (fEPSP) and field inhibitory postsynaptic potential (fIPSP) (*SI Appendix*, Fig. S3 *A*–*C*).

L-NAME instantly reduced the baseline diameter of PA, precapillary sphincter, and first-order capillaries, suggesting that constitutive NOS activity accounts for a large part of the basal vascular tone. Precapillary sphincters instantaneously exhibited stronger vasoconstriction than the PA and first-order capillaries (Fig. 2 *G*–*I*). Note that the arterial blood pressure increased from 71 ± 6 mmHg to 112 ± 25 mmHg immediately after i.v. administration of L-NAME and remained elevated for at least 30 min. This indicates that

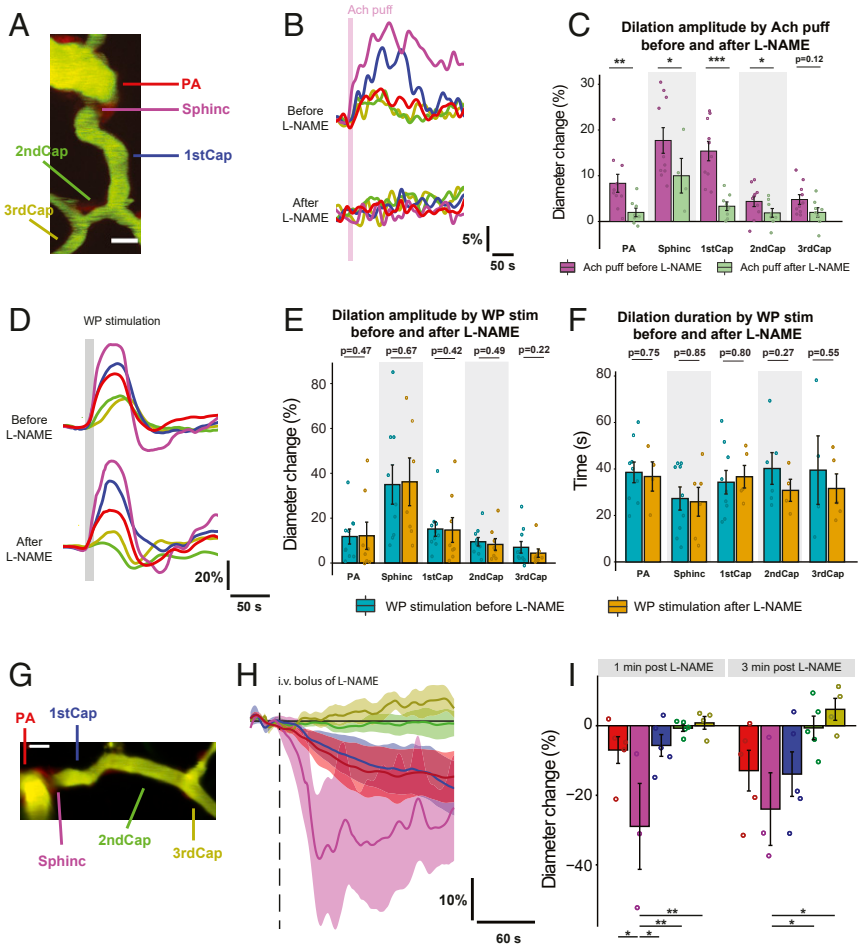

Fig. 2. Ach-induced vasodilation is mediated by NOS. (*A*) An average-projected image from a local two-photon image stack with color-coded ROIs placed across PA, precapillary sphincter (Sphinc), and first- to third-order capillaries. (Scale bar, 10 μm.) (*B*) Diameter change of the vessel segment at each ROI was estimated (*Materials and Methods*). Representative traces of Ach-puff-induced vasodilation before and after i.v. bolus infusion of L-NAME, a nonspecific NOS inhibitor. The ROIs and the trace colors are coded identically. Each trace is normalized to its mean prepuff value. (*C*) Comparison of relative diameter change at PA, precapillary sphincter (Sphinc), and first- to third-order capillaries, induced by Ach puff before and after L-NAME. Before L-NAME: $N = 5$, $n = 10$; after L-NAME: $N = 5$, $n = 8$. *N* denotes total number of animals; *n* denotes total number of vessels. (*D*) Representative traces of WP stimulation-induced vasodilation before and after L-NAME. (*E* and *F*) Comparison of WP stimulation-induced vasodilation before and after L-NAME, with (*E*) dilation amplitude and (*F*) dilation duration of half-peak. All three measurements show no significant difference. $N = 5$, $n = 5$. (*G*) An average-projected image from a local two-photon image stack with PA and first- to third-order capillaries. (*H*) Mean traces of vessel diameter change from onset of L-NAME infusion until 3 min postinfusion. $N = 5$. (*I*) Comparison of relative diameter change at PA, sphincter, and first- to third-order capillaries at 1 min and 3 min postinfusion of L-NAME. $N = 5$, $n = 5$. Linear mixed effect models were used, followed by Tukey post hoc tests. Data shown as mean ± SEM. * indicates $P < 0.05$, ** indicates $P < 0.001$, *** indicates $P < 0.0001$. (Scale bar, 10 μm.)

constitutive NOS maintain the basal vascular tone of the PA, the precapillary sphincter, and pericytes on first-order capillary and that a basal NO level is essential for preservation of capillary perfusion.

Vasodilation, Induced by the NO Donor SNAP, Is Mediated by cGMP in Capillary Pericytes. Slice experiments suggest that VSMCs on PAs are sensitive to NO, while pericytes on capillaries are not (30). To address this question directly, we puffed the NO donor S-nitroso-*N*-acetyl-DL-penicillamine (SNAP, 5 mM) onto the PA, precapillary sphincter, and first-third order capillaries and observed dilation of all segments with the largest dilator response at the precapillary sphincter (Fig. 3 *A*–*C*). This suggests that both VSMC on arterioles and pericytes on capillaries relax when exposed to NO. The receptor for NO is the soluble guanylyl cyclase (sGC), which stimulates formation of cyclic guanosine monophosphate (cGMP) that triggers smooth muscle actin relaxation (31, 32). To examine whether sGC activity in VSMCs and pericytes mediated NO-induced capillary dilation, we locally puffed SNAP before and after topical application of the specific sGC inhibitor (1H-[1,2,4]oxadiazolo-[4,3-a]quinoxalin-1-one) (ODQ) at 0.5 mM. ODQ blunted the dilator effect of SNAP in vivo (Fig. 3 *A*–*C*) and decreased pericyte calcium in vitro (*SI Appendix*, Fig. S5), which supports the hypothesis that cGMP mediates NO-induced VSMC and pericyte relaxation in brain.

Next, to examine whether cGMP participates in NVC, we compared WP-induced vasodilation before and after blocking sGC with ODQ. ODQ reduced the WP-induced vasodilator response for the PA and all capillaries, most markedly for precapillary sphincters and first-order capillaries (Fig. 3 *D* and *E*). The half-peak duration was also shortened (Fig. 3*F*). In comparison, the evoked electrical responses, fEPSP and fIPSP, remained unchanged (*SI Appendix*, Fig. S3 *D*–*F*). These results imply that modulation of sGC activity contributes to the NVC response amplitude and duration.

Pericyte K_{ATP} Channels Are Closed in Resting State and Open in Response to Increased Brain Activity. K_{ATP} channels exist in almost all cell types in the brain, including endothelial cells, VSMCs, neurons, and astrocytes. Recent findings have revealed that K_{ATP} channel expression

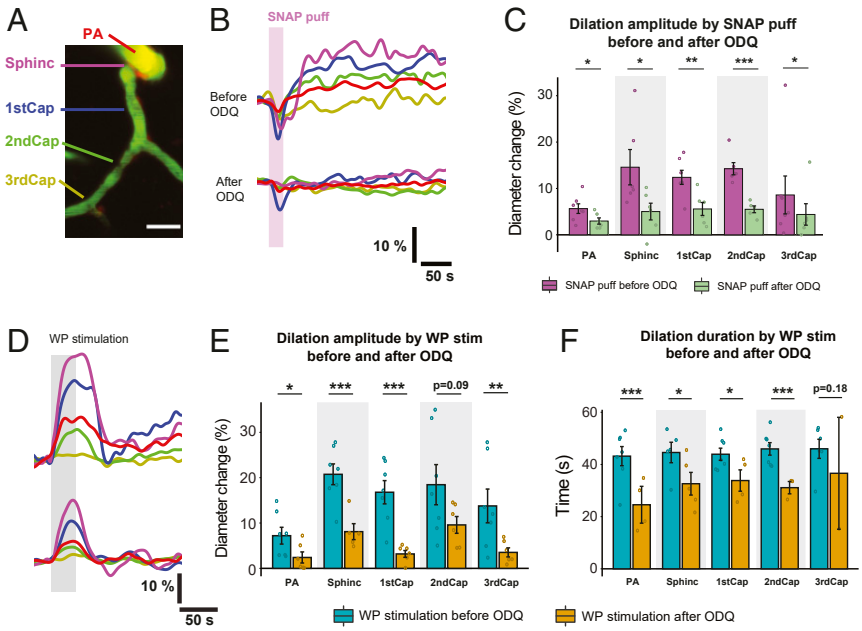

Fig. 3. NO donor SNAP-induced vasodilation is mediated by cGMP in capillary pericytes. (*A*) An average-projected image from a local two-photon image stack with PA, precapillary sphincter (Sphinc), and first- to third-order capillaries. (Scale bar, 10 μm.) (*B*) Representative traces of SNAP-puff-induced vasodilation before and after topical application of cGMP inhibitor soluble guanylyl cyclase inhibitor (ODQ). (*C*) Comparison of relative diameter change at PA, precapillary sphincter, and first- to third-order capillaries, induced by SNAP puff before and after ODQ. Before: $N = 7$, $n = 7$; after: $N = 6$, $n = 6$. *N* denotes total number of animals; *n* denotes total number of vessels. (*D–F*) Comparison of WP stimulation-induced vasodilation at PA, precapillary sphincter, and first- to third-order capillaries before and after ODQ, with (*D*) representative traces of WP stimulation-induced vasodilation before and after topical application of ODQ, (*E*) dilation amplitude, and (*F*) dilation duration of half-peak. Before: $N = 7$, $n = 7$; after: $N = 6$, $n = 6$. Linear mixed effect models were used, followed by Tukey post hoc tests. Data shown as mean ± SEM. * indicates $P < 0.05$, ** indicates $P < 0.001$, *** indicates $P < 0.0001$.

is several magnitudes higher in brain pericytes than in other cell types (21, 22), particularly in pericytes without expression of α-smooth muscle actin (αSMA) (11). This led us to examine whether pericytes K_{ATP} channels were involved in the regulation of vasodilation.

Puffing of the K_{ATP} channel opener pinacidil at 5 mM evoked dilation of PAs, precapillary sphincters, and capillaries, with the largest responses at the precapillary sphincter and first-order capillary (Fig. 4 *A–C*). This result suggested that K_{ATP} channels in VSMCs and pericytes have the potential to adjust the arteriolar and capillary diameters according to metabolic needs. In comparison, puffing of the K_{ATP} channel closer PNU37883 (PNU) at 2.5 mM or sham cerebrospinal fluid caused no significant vessel diameter change (Fig. 4 *B* and *G*), suggesting that vascular K_{ATP} channels are closed in the resting state. Topical application of 0.5 mM PNU abolished the vasodilator effect of pinacidil (Fig. 4 *A–C*), consistent with specificity of pinacidil for K_{ATP} channels.

To examine whether K_{ATP} channels were involved in NVC, we compared WP-induced vasodilation before and after topical application of 0.5 mM PNU (Fig. 4 *D–F*). This reduced the WP-induced vasodilator response amplitude (Fig. 4 *D* and *E*) and the half-peak dilation duration for PA and first- to third-order capillaries (Fig. 4*F*). These data suggested that K_{ATP} channels may maintain and prolong WP stimulation-induced vasodilation at the level of the PA, the precapillary sphincter, and first- to third-order capillaries.

To assess where in the dynamic spectrum of dilation pinacidil, Ach, and SNAP exerted their action, we compared their vasodilator responses with WP-induced vasodilation and the vascular effects of local puffing of papaverine. Papaverine relaxes VSMC by inhibiting breakdown of cGMP (33) and blocking voltage-gated calcium channels (34). The response to papaverine is commonly used to document preservation of VSMC function (25). Local puffing of 10 mM papaverine and WP stimulation triggered dilation of the PA, precapillary sphincter, and first- to third-order capillaries that was comparable to the effect of pinacidil, Ach, and SNAP, in both relative diameter change (Fig. 4*G*) and absolute change (*SI Appendix*, Fig. S4). This result suggested that pinacidil, Ach, and SNAP were appropriate for studies of vasodilator mechanisms in the PA and dilated capillaries within a physiological range.

Neither pinacidil nor PNU affected fEPSP and fIPSP responses evoked by WP stimulation (*SI Appendix*, Fig. S3 *G–L*). To rule out the possibility that calcium fluctuations in neurons and astrocytes participated in pinacidil-induced vasodilation, we examined the neuronal and astrocytic calcium responses by local bulk loading of Oregon Green BAPTA-1/AM and sulforhodamine 101 (35, 36). Pinacidil at 5 mM had no effect on neuronal or astrocytic calcium (*SI Appendix*, Fig. S6). This suggested that it is unlikely that neurons or astrocytes mediate the pinacidil response, i.e., K_{ATP} channel–mediated vasodilation.

To characterize the mechanism by which K_{ATP} channels may affect pericytes, we used in vitro experiments with pericyte monocultures from bovine brain. The in vitro data suggested that K_{ATP} channels mediate vasodilation by L-type Ca^{2+} channels in pericytes (*SI Appendix*, Fig. S7).

ET1-Induced Vasoconstriction Colocalizes with Contraction of Pericyte Somas. The potent endogenous vasoconstrictor ET1 is mainly synthesized in endothelial cells (37). ET1 expression increases in ischemia and contributes to impaired microvascular reperfusion (38, 39). We examined vascular responses to local puffing of ET1 on the PA, precapillary sphincter, and first- to third-order capillaries in vivo and in vitro. In vivo puffing of 0.5 μM ET1 instantly triggered strong vasoconstriction (Fig. 5 *A* and *B*). The constriction was long-lasting (>9 min; Fig. 5 *B* and *F*), and the most severely constricted regions of interest (ROIs) colocalized with the precapillary sphincter and pericyte somas (magenta and cyan lines) at first-order capillaries. Thus, both VSMCs on arterioles and pericytes on capillaries responded to ET1, with largest responses at precapillary sphincters in relative diameter terms and at PA and

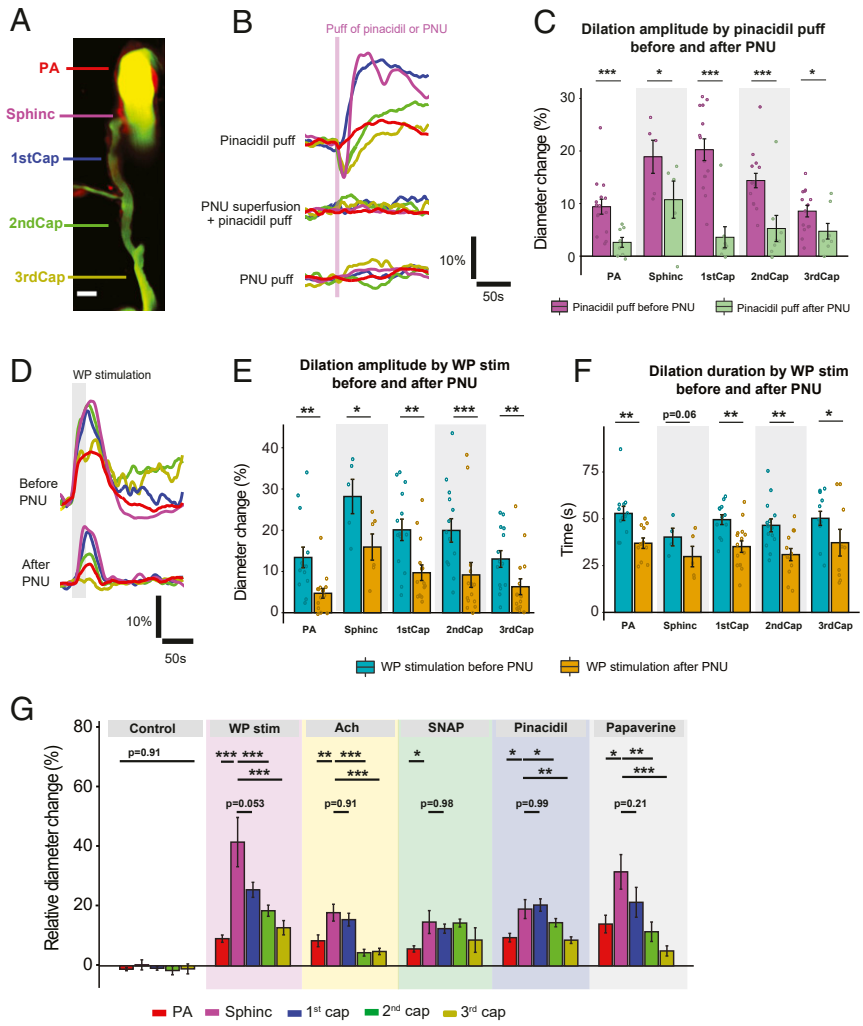

Fig. 4. K_{ATP} channels enhance and prolong WP stimulation-induced vasodilation. (*A*) An average-projected image from a local two-photon image stack with color-coded ROIs placed across at PA, precapillary sphincter (Sphinc), and first- to third-order capillaries, respectively. (Scale bar, 10 μm.) (*B*) Representative traces of K_{ATP} channel opener pinacidil puff-induced vasodilation before and after K_{ATP} channel closer PNU, as well as a trace of vascular diameter following PNU puff. (*C*) Comparison of peak diameter change in percentage. Before: $N = 9$, $n = 15$; after: $N = 5$, $n = 8$. *N* denotes total number of animals; *n* denotes total number of vessels. (*D*) Representative traces of WP stimulation-induced vasodilation before and after topical application of PNU. (*E* and *F*) Comparison of vasodilation curves before and after topical application of PNU. (*E*) Peak diameter change in percentage. Before: $N = 5$, $n = 14$; after: $N = 7$, $n = 16$. (*F*) Dilation duration between the half-peaks. (*G*) The dilation amplitudes of vessel diameter change induced by control puffing ($N = 5$), WP stimulation ($N = 8$), puffing of Ach ($N = 5$), NO donor SNAP ($N = 7$), pinacidil ($N = 9$), and papaverine ($N = 8$). Linear mixed effect models were used, followed by Tukey post hoc tests. Data shown as mean ± SEM. * indicates $P < 0.05$, ** indicates $P < 0.001$, *** indicates $P < 0.0001$.

precapillary sphincters in absolute diameter terms (Fig. 5*F* and *SI Appendix*, Fig. S4). Furthermore, preconditioning with the endothelin receptor type A antagonist BQ123 at a concentration of 0.5 mM abolished ET1-induced vasoconstriction (Fig. 5 *C*, *D*, and *F*).

Next, we asked whether ROIs with the strongest vasoconstriction also responded most strongly to vasodilator stimuli and whether this pattern of high reactivity colocalized with pericyte cell bodies. We classified the ROIs as being with or without pericyte somas but could not visualize pericyte processes because of limitations of the two-photon microscope. For both dilation and constriction, precapillary sphincters and first- and second-order capillaries with pericyte somas showed stronger reactivity to ET1 than segments without pericyte cell bodies (Fig. 5 *B*, *E*, and *G*), indicating an active role of pericytes in ET1-induced vasoconstriction. Finally, ET1 receptors did not contribute to WP stimulation-induced fEPSP and fIPSP response amplitudes (*SI Appendix*, Fig. S3 *M–O*) or vascular dilation amplitude and duration (*SI Appendix*, Fig. S8), suggesting that ET1 do not modulate NVC under normal conditions.

To assess the process of ET1-induced vasoconstriction, we examined changes in Ca^{2+} and pericyte area at cultured bovine pericytes. Opening of Ca^{2+} channels by IP_3 is assumed to be the second messenger of the ET-1 induced vasoconstriction, but whether this is the mechanism in brain pericytes is unknown. IP_3 is rapidly degraded to IP_2 and then IP_1. We measured an ET1 dose-dependent increase in IP_1, inhibitable by BQ123 (*SI Appendix*, Fig. S9) (40, 41). Our data suggested that IP_3 mediates ET1-induced pericyte constriction.

ET1 Receptor Blockers Mitigate Pericyte Contractions after Ischemia. Global ischemia is accompanied by vascular constriction within minutes, and the conventional understanding of this reaction is related to the release of vasoconstrictors from the ischemic brain. Endothelial cells may release a vasoconstrictor, as they are loaded with mitochondria and assumed to be sensitive to lack of oxygen (42). VSMCs on PAs, precapillary sphincters, and pericytes at the first- and second-order capillaries contracted instantly during the first 5 min after cardiac arrest (Fig. 6 *A*, *Upper*). Capillaries with visible pericyte somas exhibited stronger constriction than

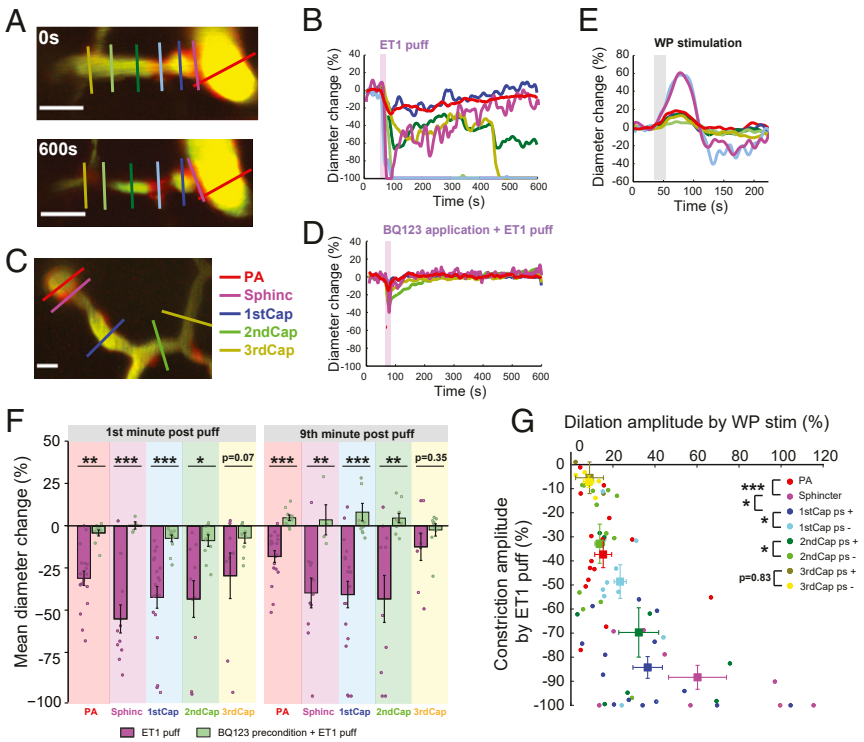

Fig. 5. ET1 induces pericyte contraction. (*A*) Representative images of 0.0005 mM ET1-puff-induced vasoconstriction. Each image is averaged from a local image stack. (*Upper*) Resting state. (*Lower*) Nine minutes after puff. (Scale bar, 20 μm.) (*B*) Normalized diameter changes over time at each color-coded ROI in *A*. (*C*) Representative image of ET1 puff after topical application of 0.5 mM BQ123 (ET1 receptor antagonist) for 45 min. (*D*) Normalized diameter changes over time at each color-coded ROI in *C*. (*E*) Vasodilation curves induced by WP stimulation at the same ROIs with *A* before ET1 puff. (*F*) Comparison of mean diameter change at 1 and 9 min after ET1 puff with or without BQ123. Without BQ123: $N = 5$, $n = 6$; with BQ123: $N = 6$, $n = 11$. *N* denotes total number of animals; *n* denotes total number of vessels. (*G*) Coregistration of ET1-induced vasoconstriction and WP stimulation-induced vasodilation at the same vessel segments (ROIs). The ROIs are classified as PA (red), precapillary sphincter (magenta), first- (blue), second- (green), and third- (yellow) order capillaries, and colocalization with pericyte soma (ps+) or without (ps−). Each dot represents an individual ROI. Error bars denote the mean ± SEM for the same color-coded ROI type. Linear mixed effect models were used, followed by Tukey post hoc tests. * indicates $P < 0.05$, ** indicates $P < 0.001$, *** indicates $P < 0.0001$. (Scale bar, 10 μm.)

capillaries lacking pericyte somas (Fig. 6*B*). The vascular pattern of ischemia-induced vasoconstriction was like that induced by ET1. This finding led us to examine whether ET1 receptors were involved. For this purpose, we topically applied to the cortex the selective ET type A-receptor antagonist BQ123 (0.5 mM) for 45 min before cardiac arrest. BQ123 mitigated the pericyte contraction in global ischemia (Fig. 6 *A*, *Lower*). The mitigation was colocalized with pericyte somas at the PA, precapillary sphincter, and first- and second-order capillaries (Fig. 6*B*). The result may imply a role for ET1 in pericyte-associated capillary constriction in global ischemia (43).

Precapillary Sphincters Are the Key Gatekeepers of Capillary Blood Flow and Pressure. Throughout our experiments we noted that the strongest microvascular responses occurred at the precapillary sphincters and first-order capillaries. To assess the possible implications of this finding we developed a mathematical model based on reconstruction of a real cerebrovascular network encompassing a PA, precapillary sphincter, and capillaries up to the sixth branching order and a penetrating venule (Fig. 7 *A* and *D*). The model assumed that flow resistances were consistent with Poiseuille's law (details in *SI Appendix* and *Materials and Methods*). This setup allowed us to calculate blood flow and pressure using Kirchoff's second law (Fig. 7 *A*, *Inset* depicts first proximal branching of the PA and associated downstream capillaries). Upon stimulation, we applied the observed diameter change in vessel segments in this study. By WP stimulation and ET1 puff, we assessed how blood flow changes correlated with relative diameter changes if individual vessel segment is disallowed from dilation/constriction. Disabling diameter change of precapillary sphincters effectively reduced the flow change by WP stimulation (Fig. 7*B*, dashed box) and ET1 puff (Fig. 7*C*, dashed box). Our result suggested that precapillary sphincters gate blood flow under conditions of activation and that precapillary sphincters are a key location to rescue in pathological conditions.

We next compared the pressure distribution in the network model under resting conditions (Fig. 7 *D*–*F*). The average pressures in the capillaries at rest (summarized in Fig. 7*E*) suggest that the precapillary sphincters must withstand more pressure than both downstream capillaries and the PA. During both WP stimulation and ET1 puff the precapillary sphincters exhibit the smallest pressure changes (Fig. 7*F*), indicating its active role to counteract local pressure fluctuation. The ability of the precapillary sphincters to produce the strongest capillary flow changes and maintain local blood pressure is expected to be matched by a large contractile capacity of precapillary sphincters. Therefore, using immunohistochemistry, we stained for αSMA, a central contractile component in vascular mural cells, to assess the relative expression in capillary pericytes and identified the strongest αSMA expression at the precapillary sphincters (Fig. 7 *G* and *H*). This finding is consistent with both the calculated pressure distribution and the observed flow changes of different capillary segments. Very low levels of αSMA were observed in third- or higher-order capillaries, consistent with these capillaries' having limited control over capillary blood flow.

Finally, we plotted the normalized pressure during WP stimulation against the normalized αSMA expression as a proxy for

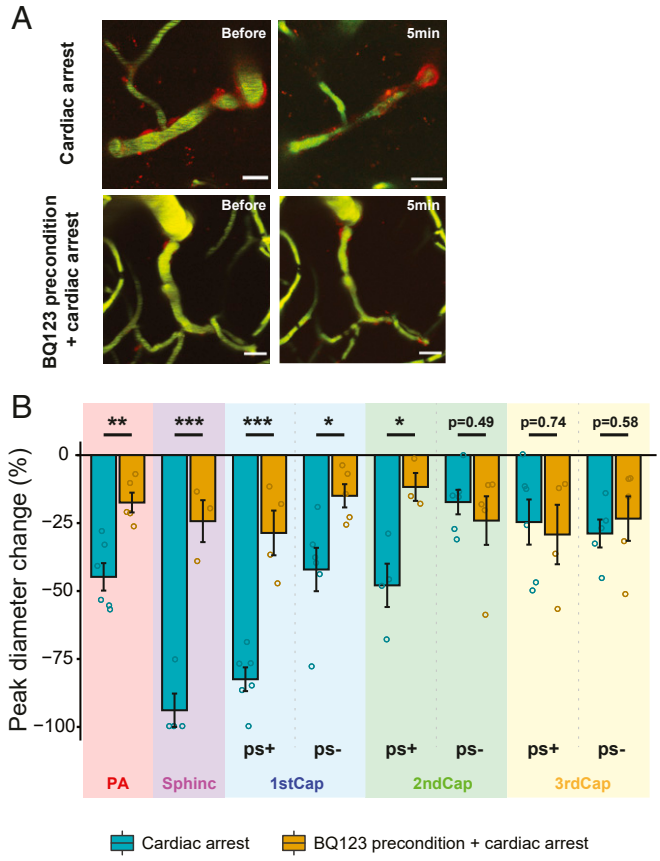

Fig. 6. Pericyte contractions after ischemia are mediated by endothelin receptors. (*A*) Representative time-lapse images of PA, precapillary sphincter, and first- to third-order capillaries under cardiac arrest induced by i.v. bolus infusion of pentobarbital. (*Upper*) Normal cardiac arrest. (*Lower*) Precondition of BQ123, which mitigated ischemia-induced pericyte constriction. (Scale bar, 20 μm.) (*B*) Summary of diameter change at PA, precapillary sphincter (Sphinc), and first- to third-order capillaries colocalized with pericyte somas or without, upon cardiac arrest with or without BQ123 precondition. ps− and ps+ denote without and with pericyte soma, respectively. Without BQ123: $N = 6$, $n = 9$; with BQ123: $N = 5$, $n = 10$. *N* denotes total number of animals; *n* denotes total number of vessels. Linear mixed effect models were used, followed by Tukey post hoc tests. Data shown as mean ± SEM. * indicates $P < 0.05$, ** indicates $P < 0.001$, *** indicates $P < 0.0001$.

force-generating ability (Fig. 7*I*). The pressure consistently correlated to the level of SMA detected in pericytes across capillary orders and was highest in precapillary sphincters, indicating that the precapillary sphincter has the highest contractile capacity of all microvessels and that this vascular segment is the key regulator of capillary blood flow under physiological conditions.

Discussion

We measured neural activity and vascular dynamics by in vivo two-photon microscopy to identify generic mechanisms underlying capillary blood flow regulation. We used 4D two-photon microscopy imaging to avoid out-of-focus challenges that are inherent to an experimental design that aims to study small movements of blood vessels in a brain that produce small movements due to the cardiac cycle and respiration. Our approach provided exceptional opportunities for 3D, spatiotemporal resolution of microvascular reactivity.

Our study shows that 1) capillary blood flow is regulated primarily by precapillary sphincters and pericytes at first-order capillaries as a result of higher expression of αSMA than at downstream capillaries; 2) capillary endothelial cells contribute to arteriolar and capillary vascular tone via the NO-cGMP pathway; 3) activation of K_{ATP} channels produces vasodilation mainly of precapillary sphincters and enhances and prolongs the NVC response; and 4) the mechanism underlying activation of K_{ATP} channels is associated with closing of L-type Ca^{2+} channels at pericyte membranes. Furthermore, we show that 5) ET1-induced pericyte contraction occurred at the pericyte soma, via IP_3 signaling and 6) ET1 contributes to the constriction observed following cardiac arrest. In summary, we report stimulation-induced rises in blood flow, i.e., NVC, and vascular responses to a suite of vasoactive molecules that dilate both PAs and brain capillaries.

In this study we mainly focused on contractile mural cells located at arterioles and their initial branches of capillaries. Although the examined first- to third-order capillaries are likely covered by ensheathing pericytes (*SI Appendix*, Fig. S1) (44), there is no staining of αSMA in NG2DsRed mice and therefore it is impossible to securely determine pericyte subtypes. Thus, we used the unbiased, unambiguous vascular branch order to identify pericytes. Pericytes without expression of αSMA (αSMA−) locate at higher-order capillaries, where functional vasodilation is preceded by pericytes at the first few order capillaries with expression of αSMA (αSMA+) (44, 45). However, this does not rule out the contribution of αSMA pericytes for basal capillary flow resistance (44, 46), as well as their involvement of sensing local activity and conveying them retrograde to upstream arterioles that induce vasodilation (20).

In big arteries and arterioles the NO/cGMP signaling cascade mediates endothelium-dependent relaxation of smooth muscle cells (47). Here, we demonstrate that the NO/cGMP pathway is a signaling pathway from endothelium to pericytes in brain capillaries; however, we did not confirm a primary involvement of the pathway in NVC. These results are consistent with studies in rats (48, 49) and some results obtained in mice (4), but other mouse studies have shown that NVC may be curtailed by L-NAME infusion in wild-type and eNOS knockout mice (50). The discrepancy could trace to different species or strains (rats versus mice and different mouse strains) or locations (capillaries in our study versus previous reports on artery/arterioles).

The NO-cGMP pathway modulates rather than mediates NVC in the somatosensory cortex (51). Therefore, the absence of an L-NAME effect may be consistent with a greater relevance of other modulators. In comparison, blocking cGMP synthesis with ODQ led to a decrease of the NVC dilation response and duration (52). This result could suggest that NO is not the only activator of the sGC. Alternatively, CO is also able to activate sGC and a potential mediator of NVC (53, 54). Furthermore, L-NAME is expected to penetrate the blood–brain barrier along paracellular pathways and inhibit NOS in interneurons (28, 55–57). However, no studies so far have separated NOS in nerve cells and endothelial cells when assessing the effect of L-NAME on crude brain extracts (57, 58). In our current study, L-NAME did not affect NVC, but both subtypes of NOS (endothelial NOS and neuronal NOS) may contribute to maintain the basal vascular tone. I.v. L-NAME blocked the vasodilation induced by Ach, which is the commonly used molecule to assess endothelial–VSMC interaction by rises in constitutive eNOS activity.

NOS activity differs among brain regions; it is high in the cerebellum and low in the cerebral cortex (59). In brain slice experiments it was shown that upon glutamate superfusion (a proxy for functional stimulation) cerebellar capillary dilation is mediated by pericytes and is NO-dependent (8). However, ODQ does not inhibit the NO-dependent capillary diameter increase caused by glutamate, indicating that NO does not act by raising [cGMP] in the pericytes in cerebellum (8). In contrast, cerebral cortical capillary dilation induced by neuronal activation evoked by direct cortical electrical stimulation is not affected by NO-synthase inhibition, implying that NO does not contribute to capillary dilation in cerebral cortex (30). These results demonstrate that there might be differences in signaling mechanisms of the NVC among brain

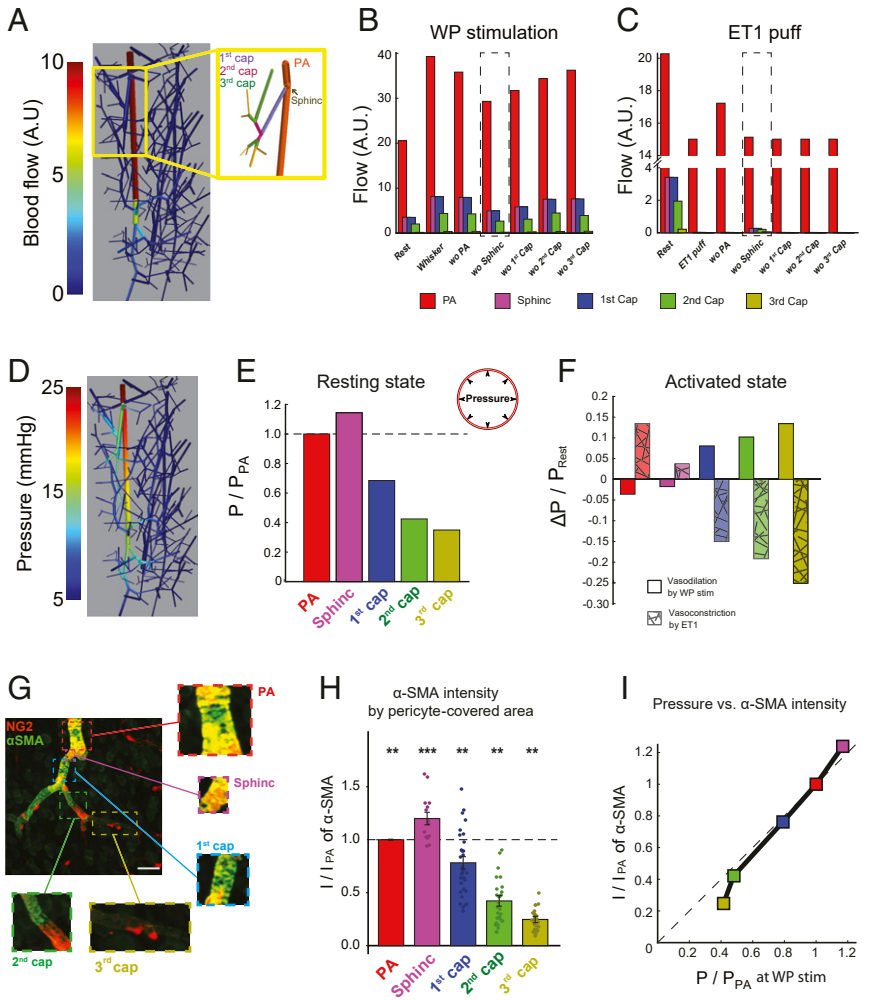

Fig. 7. Precapillary sphincters are the key gatekeepers of capillary blood flow. (*A*) Mathematical modeling of flow distribution in a reconstructed cerebrovascular tree containing one PA and venule (*Materials and Methods*), under resting conditions. (*B*) Summary of calculated average blood flows among all PA, precapillary sphincter (Sphinc), and first- to third-order capillary segments in the network before (Rest) and during WP stimulation. The groups labeled with "wo" denote calculations of WP stimulations in which either the PA, precapillary sphincter, and first- to third-order capillary segments were disallowed from dilating. Note the precapillary sphincter has the strongest influence on network flows, as shown in the dashed box. (*C*) Summary of calculated blood flows in the vessel segments before (Rest) and during ET1 puff. Similar to *B*, calculations of the puff where segments were disallowed from constricting are shown in the "wo"-labeled groups. A.U., arbitrary units. (*D*) Mathematical modeling of pressure distribution in the resting state. Inlet pressure into the PA was set to 25 mmHg, whereas all outlet pressures were set to 5 mmHg. (*E*) Summary of the average pressures in PA, precapillary sphincter, and first- to third-order capillaries in the network normalized to the average pressure in the PA. (*F*) Normalized pressure change at PA, precapillary sphincter, and first- to third-order capillaries by dilation or constriction. (*G*) Representative image of mural cells (red) and αSMA (green) staining among the PA (red inset), precapillary sphincter (magenta inset), first-order capillaries (blue inset), second-order capillaries (green insert), and third-order capillaries (orange inset); see insets for enlargements. (*H*) Summarized intensity of αSMA in pericytes on precapillary sphincter and first-, second-, or third-order capillaries normalized to the intensity from αSMA intensity on the PA. Note that αSMA is significantly more expressed in precapillary sphincters than PA and first- to third-order capillaries, whereas all first- to third-order capillaries contained less αSMA than PA. Individual vessel segments are compared to all other vessel segments, and the highest *P* value is illustrated. $N = 3$, $n = 31$. *N* denotes total number of animals; *n* denotes total number of vessels. Linear mixed effect models were used, followed by Tukey post hoc tests. Data shown as mean ± SEM. (*I*) Relationship between normalized pressure and normalized αSMA density at peak dilation upon WP stimulation. * indicates $P < 0.05$, ** indicates $P < 0.001$, *** indicates $P < 0.0001$.

regions. Our in vivo results are at variance with some of these findings; these differences may be caused by differences in stimulation protocols, different preparations (in vivo versus in vitro), differences in studied brain location, or different breeds or species of experimental animals.

K_{ATP} channels exist in almost all cell types in the brain and abound in brain pericytes (21, 22). Moreover, single-cell transcriptomic data showed that K_{ATP} channel gene expression (kcnj8 and abcc9) is much higher in αSMA-capillary pericytes, compared with αSMA+ mural cells (11). Although pinacidil puffing may possibly induce a direct local pericyte relaxation, it is also likely that our observation of pinacidil-induced vasodilation was caused by hyperpolarization of higher-order capillary pericytes and retrograde conduction of the dilatory signal along the capillaries. K_{ATP} channels are sensitive to CBF and parenchymal oxygen partial pressure (60) and may be neuroprotective during ischemia and hypoxia (61). Pericyte K_{ATP} channels on freshly isolated retinal microvessels open in response to adenosine receptor activation (62), and in the retina most K_{ATP} channel-generated currents are in mural cells of capillaries (63). Our findings suggest that K_{ATP} channels in pericytes enhance and prolong the vasodilator response to increases in brain activity. Similar to VSMCs, the signaling pathway involves potassium outflow

and membrane hyperpolarization, which inactivates L-type Ca^{2+} channels and leads to vasodilation through reduced intracellular Ca^{2+} (64). Further, functional pericyte L-type Ca^{2+} channels, in regard to pericyte Ca^{2+} signaling and constriction, were recently demonstrated in retinal preparations (65).

The potent endogenous vasoconstrictor endothelin is synthesized in endothelial cells, and in brain the endothelin type A receptor is only expressed in vascular mural cells (37). Mural cell endothelin type A receptors are activated by paracrine endothelin signaling, and the basal vascular tone and blood pressure are determined to some extent by the balance between secreted NO and endothelin (66). Numerous pathological factors stimulate endothelial cells to produce endothelin, e.g., inflammation, ischemia, and reactive oxygen species (37, 67). In comparison, NO, PGE_2, and PGI_2 suppress the translation and secretion of endothelin (68, 69). Therefore, our results of ET1-mediated vascular constriction is mainly relevant for brain pathology.

Fluctuations in intracellular calcium activity of pericytes regulate contractility and the capillary diameter (45), but in the present work we examined several vasodilators and constrictors that were expected to modulate additional intracellular messenger molecules. Therefore, we decided to carry out a series of in vitro experiments using cultured pericytes in parallel to the in vivo experiments to identify second messengers that change in response to application of vasoactive substances while at the same time we recorded pericyte contraction or relaxation reflecting their content of αSMA. Our in vitro data suggest that K_{ATP} channels mediate vasodilation by L-type Ca^{2+} channels in pericytes, and ET1 channels mediate vasoconstriction via IP_3 in pericytes. Our results are supported by a recent pericyte Ca^{2+} imaging study in retinal preparation that showed increases in pericyte Ca^{2+} upon administration of membrane permeable IP_3 analog Bt-IP_3 (65).

In the last part of our study we asked why the precapillary sphincters generated the largest response to both systemic infusion of L-NAME, neurotransmitter-mediated signaling, and vasoactive molecules (pinacidil, papaverine, Ach, SNAP, and ET1). This led us to hypothesize that intrinsic properties of precapillary sphincters were particularly important for their reactivity. We show that αSMA expression at precapillary sphincters was more abundant than at VSMCs at the PA, as well as more abundant than pericytes at first- to third-order capillaries. This pattern of αSMA expression fits with the modeled pressure profile among vessel segments. The arterial pressure head in the systole is strong at the PA, which must be able to produce a great force in order to maintain a near-constant perfusion pressure. Indeed, the pressure distribution in a reconstructed vascular network matched αSMA expression (Fig. 7). The model also assessed how blood flow may be distributed among the PA, precapillary sphincters, and first-, second-, and third-order capillaries with diameter changes of each vessel segment. During both vasodilation and vasoconstriction capillary blood flow changes are dramatically blunt if disabling precapillary sphincter diameter change. In comparison, diameter changes in second- or higher-order capillaries are mainly passive and of little consequence for capillary flow. Our data agree with previous studies that detected αSMA in pericytes up to the third to fourth order of capillaries and with the notion that pericyte regulation of capillaries is mechanistically related to αSMA contraction and relaxation (10).

In summary, our 4D two-photon imaging data provide mechanistic insight to the integrated vascular function that regulates brain capillary blood flow. Our results reveal a key role for precapillary sphincters and pericytes at first-order capillaries for blood flow control, which may have translational implications for a better understanding of cerebrovascular and neurodegenerative disorders and functional neuroimaging.

Materials and Methods

In vivo 4D (x–y–z–t) two-photon microscopy was used to image the somatosensory cortex of anesthetized NG2dsRed mice (Fig. 1 *A* and *B*), which express a red fluorescent protein in pericytes (Fig. 1*C*) and in VSMCs. FITC-dextran was applied i.v. to stain the vessel lumen green. WP stimulation was used to activate the somatosensory cortex and elicit functional hyperemia. Borosilicate glass micropipettes with a resistance of 3 to 3.5 MΩ were loaded with a mixture of vasoactive substances and 10 μM Alexa 594 for local pressure ejection (puff) of vasoactive compounds and for recording of local field potentials (Fig. 1 *A*–*C*). All data are presented as means ± SEM. *N* denotes total number of animals; *n* denotes total number of vasculatures. Statistical analysis of a linear mixed-effects model followed by Tukey post hoc tests was used for the in vivo dataset. A detailed description of the materials and methods is provided in *SI Appendix*. The data that support the findings of this study are provided as source data files. All procedures were approved by the Danish National Ethics Committee according to the guidelines set forth in the European Council's Convention for the Protection of Vertebrate Animals used for Experimental and Other Scientific Purposes and are in compliance with the ARRIVE guidelines.

Data Availability. Excel data have been deposited in G-Node (DOI: 10.12751/g-node.vi9c1i).

ACKNOWLEDGMENTS. We acknowledge Dr. Søren Grubb, Dr. Krzysztof Kucharz, Dr. Henrik Flyvbjerg, Dr. Barbara Lind, and Dr. Nikolay Kutuzov for scientific discussions. We also acknowledge Dr. Søren Grubb for providing the z-stack for our modeling work. We acknowledge the Core Facility for Integrated Microscopy, Faculty of Health and Medical Sciences, University of Copenhagen, where we used confocal and spinning disc confocal microscopy in our in vitro studies. We further acknowledge Dr. Thor Møller for introduction to and assistance with the IP-one assay. This study was supported by the Lundbeck Foundation, the Danish Medical Research Council, the Alice Brenaa Foundation, Augustinus Foundation, Carl og Ellen Hertz Familielegat, the NOVO Nordisk Foundation, and a Nordea Foundation grant to the Center for Healthy Aging.

1. M. E. Raichle, D. A. Gusnard, Appraising the brain's energy budget. *Proc. Natl. Acad. Sci. U.S.A.* **99**, 10237–10239 (2002).
2. D. Attwell *et al.*, Glial and neuronal control of brain blood flow. *Nature* **468**, 232–243 (2010).
3. C. Iadecola, The neurovascular unit coming of age: A journey through neurovascular coupling in health and disease. *Neuron* **96**, 17–42 (2017).
4. B. W. Chow *et al.*, Caveolae in CNS arterioles mediate neurovascular coupling. *Nature* **579**, 106–110 (2020).
5. Z. Arvanitakis, A. W. Capuano, S. E. Leurgans, D. A. Bennett, J. A. Schneider, Relation of cerebral vessel disease to Alzheimer's disease dementia and cognitive function in elderly people: A cross-sectional study. *Lancet Neurol.* **15**, 934–943 (2016).
6. J. H. Zhang *et al.*, The vascular neural network–A new paradigm in stroke pathophysiology. *Nat. Rev. Neurol.* **8**, 711–716 (2012).
7. J. H. van Lieshout *et al.*, An introduction to the pathophysiology of aneurysmal subarachnoid hemorrhage. *Neurosurg. Rev.* **41**, 917–930 (2018).
8. C. N. Hall *et al.*, Capillary pericytes regulate cerebral blood flow in health and disease. *Nature* **508**, 55–60 (2014).
9. C. Cai *et al.*, Stimulation-induced increases in cerebral blood flow and local capillary vasoconstriction depend on conducted vascular responses. *Proc. Natl. Acad. Sci. U.S.A.* **115**, E5796–E5804 (2018).
10. R. I. Grant *et al.*, Organizational hierarchy and structural diversity of microvascular pericytes in adult mouse cortex. *J. Cereb. Blood Flow Metab.* **39**, 411–425 (2019).
11. M. Vanlandewijck *et al.*, A molecular atlas of cell types and zonation in the brain vasculature. *Nature* **554**, 475–480 (2018).
12. D. Attwell, A. Mishra, C. N. Hall, F. M. O'Farrell, T. Dalkara, What is a pericyte? *J. Cereb. Blood Flow Metab.* **36**, 451–455 (2016).
13. K. Kisler, A. R. Nelson, A. Montagne, B. V. Zlokovic, Cerebral blood flow regulation and neurovascular dysfunction in Alzheimer disease. *Nat. Rev. Neurosci.* **18**, 419–434 (2017).
14. A. R. Nelson *et al.*, Channelrhodopsin excitation contracts brain pericytes and reduces blood flow in the aging mouse brain *in vivo*. *Front. Aging Neurosci.* **12**, 108 (2020).
15. L. Khennouf *et al.*, Active role of capillary pericytes during stimulation-induced activity and spreading depolarization. *Brain* **141**, 2032–2046 (2018).
16. K. Kisler *et al.*, Pericyte degeneration leads to neurovascular uncoupling and limits oxygen supply to brain. *Nat. Neurosci.* **20**, 406–416 (2017).
17. B. R. Chen, M. G. Kozberg, M. B. Bouchard, M. A. Shaik, E. M. Hillman, A critical role for the vascular endothelium in functional neurovascular coupling in the brain. *J. Am. Heart Assoc.* **3**, e000787 (2014).
18. A. D. Hogan-Cann, P. Lu, C. M. Anderson, Endothelial NMDA receptors mediate activity-dependent brain hemodynamic responses in mice. *Proc. Natl. Acad. Sci. U.S.A.* **116**, 10229–10231 (2019).
19. T. A. Longden, M. T. Nelson, Vascular inward rectifier K+ channels as external K+ sensors in the control of cerebral blood flow. *Microcirculation* **22**, 183–196 (2015).
20. T. A. Longden *et al.*, Capillary K^+-sensing initiates retrograde hyperpolarization to increase local cerebral blood flow. *Nat. Neurosci.* **20**, 717–726 (2017).

21. S. Chasseigneaux *et al*., Isolation and differential transcriptome of vascular smooth muscle cells and mid-capillary pericytes from the rat brain. *Sci. Rep.* **8**, 12272 (2018).
22. L. He *et al*., Analysis of the brain mural cell transcriptome. *Sci. Rep.* **6**, 35108 (2016).
23. D. A. Hartmann, R. G. Underly, A. N. Watson, A. Y. Shih, A murine toolbox for imaging the neurovascular unit. *Microcirculation* **22**, 168–182 (2015).
24. C. Cai *et al*., In vivo three-dimensional two-photon microscopy to study conducted vascular responses by local ATP ejection using a glass micro-pipette. *J. Vis. Exp.*, 10.3791/59286 (2019).
25. W. I. Rosenblum, Endothelium-dependent responses in the microcirculation observed in vivo. *Acta Physiol. (Oxf.)* **224**, e13111 (2018).
26. E. A. Winkler, R. D. Bell, B. V. Zlokovic, Central nervous system pericytes in health and disease. *Nat. Neurosci.* **14**, 1398–1405 (2011).
27. B. M. Radu *et al*., All muscarinic acetylcholine receptors (M_1-M_5) are expressed in murine brain microvascular endothelium. *Sci. Rep.* **7**, 5083 (2017).
28. M. Fabricius, I. Rubin, M. Bundgaard, M. Lauritzen, NOS activity in brain and endothelium: Relation to hypercapnic rise of cerebral blood flow in rats. *Am. J. Physiol.* **271**, H2035–H2044 (1996).
29. C. Iadecola, J. Li, T. J. Ebner, X. Xu, Nitric oxide contributes to functional hyperemia in cerebellar cortex. *Am. J. Physiol.* **268**, R1153–R1162 (1995).
30. A. Mishra *et al*., Astrocytes mediate neurovascular signaling to capillary pericytes but not to arterioles. *Nat. Neurosci.* **19**, 1619–1627 (2016).
31. G. Filippov, D. B. Bloch, K. D. Bloch, Nitric oxide decreases stability of mRNAs encoding soluble guanylate cyclase subunits in rat pulmonary artery smooth muscle cells. *J. Clin. Invest.* **100**, 942–948 (1997).
32. W. S. Scott, D. K. Nakayama, Sustained nitric oxide exposure decreases soluble guanylate cyclase mRNA and enzyme activity in pulmonary artery smooth muscle. *J. Surg. Res.* **79**, 66–70 (1998).
33. V. Boswell-Smith, D. Spina, C. P. Page, Phosphodiesterase inhibitors. *Br. J. Pharmacol.* **147** (suppl. 1), S252–S257 (2006).
34. T. B. Bolton, Mechanisms of action of transmitters and other substances on smooth muscle. *Physiol. Rev.* **59**, 606–718 (1979).
35. J. C. Fordsmann *et al*., Spontaneous astrocytic Ca^{2+} activity abounds in electrically suppressed ischemic penumbra of aged mice. *Glia* **67**, 37–52 (2019).
36. B. L. Lind *et al*., Fast Ca^{2+} responses in astrocyte end-feet and neurovascular coupling in mice. *Glia* **66**, 348–358 (2018).
37. A. P. Davenport *et al*., Endothelin. *Pharmacol. Rev.* **68**, 357–418 (2016).
38. I. Ziv *et al*., Increased plasma endothelin-1 in acute ischemic stroke. *Stroke* **23**, 1014–1016 (1992).
39. H. Han, S. Neubauer, B. Braeker, G. Ertl, Endothelin-1 contributes to ischemia/reperfusion injury in isolated rat heart-attenuation of ischemic injury by the endothelin-1 antagonists BQ123 and BQ610. *J. Mol. Cell. Cardiol.* **27**, 761–766 (1995).
40. E. Trinquet *et al*., D-myo-inositol 1-phosphate as a surrogate of D-myo-inositol 1,4,5-tris phosphate to monitor G protein-coupled receptor activation. *Anal. Biochem.* **358**, 126–135 (2006).
41. E. Trinquet, R. Bouhelal, M. Dietz, Monitoring Gq-coupled receptor response through inositol phosphate quantification with the IP-One assay. *Expert Opin. Drug Discov.* **6**, 981–994 (2011).
42. D. W. Busija, P. V. Katakam, Mitochondrial mechanisms in cerebral vascular control: Shared signaling pathways with preconditioning. *J. Vasc. Res.* **51**, 175–189 (2014).
43. A. Ames III, R. L. Wright, M. Kowada, J. M. Thurston, G. Majno, Cerebral ischemia. II. The no-reflow phenomenon. *Am. J. Pathol.* **52**, 437–453 (1968).
44. D. A. Hartmann *et al*., Brain capillary pericytes exert a substantial but slow influence on blood flow. *Nat. Neurosci.* **24**, 633–645 (2021).
45. R. L. Rungta, E. Chaigneau, B. F. Osmanski, S. Charpak, Vascular compartmentalization of functional hyperemia from the synapse to the pia. *Neuron* **99**, 362–375.e4 (2018).
46. P. Blinder *et al*., The cortical angiome: An interconnected vascular network with noncolumnar patterns of blood flow. *Nat. Neurosci.* **16**, 889–897 (2013).
47. A. Sandoo, J. J. van Zanten, G. S. Metsios, D. Carroll, G. D. Kitas, The endothelium and its role in regulating vascular tone. *Open Cardiovasc. Med. J.* **4**, 302–312 (2010).
48. Q. Wang *et al*., Nitric oxide does not act as a mediator coupling cerebral blood flow to neural activity following somatosensory stimuli in rats. *Neurol. Res.* **15**, 33–36 (1993).
49. K. Adachi *et al*., Increases in local cerebral blood flow associated with somatosensory activation are not mediated by NO. *Am. J. Physiol.* **267**, H2155–H2162 (1994).
50. P. Toth *et al*., Purinergic glio-endothelial coupling during neuronal activity: Role of P2Y1 receptors and eNOS in functional hyperemia in the mouse somatosensory cortex. *Am. J. Physiol. Heart Circ. Physiol.* **309**, H1837–H1845 (2015).
51. U. Lindauer, D. Megow, H. Matsuda, U. Dirnagl, Nitric oxide: A modulator, but not a mediator, of neurovascular coupling in rat somatosensory cortex. *Am. J. Physiol.* **277**, H799–H811 (1999).
52. M. Kuhn, Molecular physiology of membrane guanylyl cyclase receptors. *Physiol. Rev.* **96**, 751–804 (2016).
53. A. Friebe, G. Schultz, D. Koesling, Sensitizing soluble guanylyl cyclase to become a highly CO-sensitive enzyme. *EMBO J.* **15**, 6863–6868 (1996).
54. J. A. Filosa, H. W. Morrison, J. A. Iddings, W. Du, K. J. Kim, Beyond neurovascular coupling, role of astrocytes in the regulation of vascular tone. *Neuroscience* **323**, 96–109 (2016).
55. N. A. Ayers, L. Kapás, J. M. Krueger, The inhibitory effects of N omega-nitro-L-arginine methyl ester on nitric oxide synthase activity vary among brain regions in vivo but not in vitro. *Neurochem. Res.* **22**, 81–86 (1997).
56. C. Iadecola, X. Xu, F. Zhang, J. Hu, E. E. el-Fakahany, Prolonged inhibition of brain nitric oxide synthase by short-term systemic administration of nitro-L-arginine methyl ester. *Neurochem. Res.* **19**, 501–505 (1994).
57. R. J. Traystman *et al*., Nitro-L-arginine analogues. Dose- and time-related nitric oxide synthase inhibition in brain. *Stroke* **26**, 864–869 (1995).
58. M. Fabricius, M. Lauritzen, Laser-Doppler evaluation of rat brain microcirculation: Comparison with the [14C]-iodoantipyrine method suggests discordance during cerebral blood flow increases. *J. Cereb. Blood Flow Metab.* **16**, 156–161 (1996).
59. M. Salter, C. Duffy, J. Garthwaite, P. J. Strijbos, Substantial regional and hemispheric differences in brain nitric oxide synthase (NOS) inhibition following intracerebroventricular administration of N omega-nitro-L-arginine (L-NA) and its methyl ester (L-NAME). *Neuropharmacology* **34**, 639–649 (1995).
60. P. S. Hosford *et al*., A critical role for the ATP-sensitive potassium channel subunit $K_{IR}6.1$ in the control of cerebral blood flow. *J. Cereb. Blood Flow Metab.* **39**, 2089–2095 (2019).
61. V. Szeto, N. H. Chen, H. S. Sun, Z. P. Feng, The role of K_{ATP} channels in cerebral ischemic stroke and diabetes. *Acta Pharmacol. Sin.* **39**, 683–694 (2018).
62. Q. Li, D. G. Puro, Adenosine activates ATP-sensitive K(+) currents in pericytes of rat retinal microvessels: Role of A1 and A2a receptors. *Brain Res.* **907**, 93–99 (2001).
63. E. Ishizaki, M. Fukumoto, D. G. Puro, Functional K(ATP) channels in the rat retinal microvasculature: Topographical distribution, redox regulation, spermine modulation and diabetic alteration. *J. Physiol.* **587**, 2233–2253 (2009).
64. T. P. Flagg, D. Enkvetchakul, J. C. Koster, C. G. Nichols, Muscle KATP channels: Recent insights to energy sensing and myoprotection. *Physiol. Rev.* **90**, 799–829 (2010).
65. A. L. Gonzales *et al*., Contractile pericytes determine the direction of blood flow at capillary junctions. *Proc. Natl. Acad. Sci. U.S.A.* **117**, 27022–27033 (2020).
66. R. M. Rapoport, Acute nitric oxide synthase inhibition and endothelin-1-dependent arterial pressure elevation. *Front. Pharmacol.* **5**, 57 (2014).
67. L. R. Stow, M. E. Jacobs, C. S. Wingo, B. D. Cain, Endothelin-1 gene regulation. *FASEB J.* **25**, 16–28 (2011).
68. B. A. Prins *et al*., Prostaglandin E2 and prostacyclin inhibit the production and secretion of endothelin from cultured endothelial cells. *J. Biol. Chem.* **269**, 11938–11944 (1994).
69. S. L. Bourque, S. T. Davidge, M. A. Adams, The interaction between endothelin-1 and nitric oxide in the vasculature: New perspectives. *Am. J. Physiol. Regul. Integr. Comp. Physiol.* **300**, R1288–R1295 (2011).